

The reactivity of $[\text{ReBr}_3(\text{MeCN})(\text{dppe})]$ towards gaseous nitric oxide. The X-ray structure of $[\text{ReBr}_3(\text{MeCN})(\text{dppe})]$ and $[\text{ReBr}_3(\text{NO})(\text{dppe})]_{0.57}[\text{ReOBr}_3(\text{dppe})]_{0.43}$ and DFT calculations for $[\text{ReBr}_3(\text{NO})(\text{dppe})]$ and $[\text{ReOBr}_3(\text{dppe})]$

B. Machura^{a,*}, R. Kruszynski^b, M. Jaworska^c

^aDepartment of Inorganic and Radiation Chemistry, Institute of Chemistry, University of Silesia, 9th Szkolna Street, 40-006 Katowice, Poland

^bX-ray Crystallography Laboratory, Institute of General and Ecological Chemistry, Technical University of Łódź, 116 Żeromski Street, 90-924 Łódź, Poland

^cDepartment of Theoretical Chemistry, Institute of Chemistry, University of Silesia, 9th Szkolna Street, 40-006 Katowice, Poland

Received 18 November 2004; revised 17 January 2005; accepted 17 January 2005

Abstract

The $[\text{ReOBr}_3(\text{dppe})]$ ($\text{dppe} = \text{bis}(\text{diphenylphosphino})\text{ethane}$) complex reacts with acetonitrile in the presence of excess of triphenylphosphine to give a new monomeric rhenium(III) complex— $[\text{ReBr}_3(\text{MeCN})(\text{dppe})]$ (**1**). The reaction of **1** with gaseous nitric oxide leads to the mixed $[\text{ReBr}_3(\text{NO})(\text{dppe})]_{0.57}[\text{ReOBr}_3(\text{dppe})]_{0.43}$ complex (**2**) with rhenium atoms on +2 and +5 oxidation states. This paper presents the synthesis, spectroscopic characterisation and X-ray structure of **1** and **2**. The geometries of $[\text{ReBr}_3(\text{NO})(\text{dppe})]$ and $[\text{ReOBr}_3(\text{dppe})]$ have been optimized using the density functional theory (DFT) and the electronic transitions of $[\text{ReBr}_3(\text{NO})(\text{dppe})]$ and $[\text{ReOBr}_3(\text{dppe})]$ have been calculated with the time-dependent DFT method (TDDFT). The UV–vis spectrum of **2** has been interpreted on the basis of the experimental data for $[\text{ReOBr}_3(\text{dppe})]$ and the calculated transitions for $[\text{ReOBr}_3(\text{dppe})]$ and $[\text{Re}(\text{NO})\text{Br}_3(\text{dppe})]$.

© 2005 Elsevier B.V. All rights reserved.

Keywords: Rhenium; Acetonitrile; Nitric oxide; Nitrosyl complexes; DFT and TDDFT calculations

1. Introduction

The nitrile complexes have been recognized as convenient substrates in the syntheses of organometallic derivatives for many years. The $\text{R}-\text{C}\equiv\text{N}$ ligands can be readily displaced by other isoelectronic unsaturated ligands such as dinitrogen, carbon monoxide, isocyanides and alkynes [1–5] or can be converted into other organic ligands in such chemical processes as insertion and nucleophilic or electrophilic attack [1,6–9].

The main aim of the paper was the preparation of the nitrile rhenium complex with bis(diphenylphosphino)ethane (dppe) in coordination sphere and using it to

a synthesis of rhenium nitrosyls. Previously, we reported the structural and spectroscopic characterisation of the nitrosyl rhenium complexes obtained in the reactions of the $[\text{ReOX}_3\text{L}_2]$ complexes ($\text{X} = \text{Cl}, \text{Br}$ and $\text{L} = \text{PPh}_3, \text{AsPh}_3, 1/2 \text{ dppe}$ and $1/2 \text{ bipy}$) with gaseous nitric oxide [10–21].

The finding that $[\text{ReCl}_3(\text{PPh}_3)_2]$, generated in situ from $[\text{ReOCl}_3(\text{PPh}_3)_2]$ and PPh_3 , undergoes a direct reaction with the triazenido anion $\text{Li}(\text{RN}=\text{N}=\text{NR})$ to give *trans*- $[\text{ReCl}_2(\text{PPh}_3)_2(\text{RN}=\text{N}=\text{NR})]$ [22], prompted us to explore the reaction of $[\text{ReOBr}_3(\text{dppe})]$ with acetonitrile in the presence of excess of triphenylphosphine as a direct route to the nitrile complex.

The $[\text{ReBr}_3(\text{MeCN})(\text{dppe})]$ complex (**1**) obtained in the above method, reacts with gaseous nitric oxide to give $[\text{ReBr}_3(\text{NO})(\text{dppe})]_{0.57}[\text{ReOBr}_3(\text{dppe})]_{0.43}$ (**2**). Here we present the synthesis, spectroscopic characterisation

* Corresponding author. Tel.: +48 322582441; fax: +48 322599978.

E-mail addresses: basia@ich.us.edu.pl (B. Machura), mj@ich.us.edu.pl (M. Jaworska).

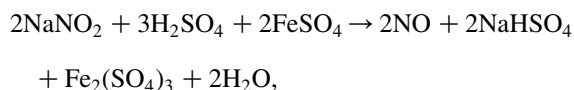
and X-ray structure of **1** and **2**. The UV–vis spectrum of **2** has been discussed on the basis of the experimental data for [ReOBr₃(dppe)] and the calculated transitions for [ReOBr₃(dppe)] and [Re(NO)Br₃(dppe)]. The geometries of [ReOBr₃(dppe)] and [Re(NO)Br₃(dppe)] have been optimised with the density functional theory (DFT) and their electronic spectra have been calculated with the time-dependent DFT method (TDDFT).

The calculations with TDDFT method for closed-shell and open-shell organic, inorganic and organometallic molecules (including 5d-metal complexes) are still limited but a few studies have already appeared and supported the TDDFT method to be applicable for such systems giving good assignment of experimental spectra [23–34].

2. Experimental

Triphenylphosphine, bis(diphenylphosphino)ethane and ammonium perchlorate were purchased from Aldrich Chemical Co. and used without further purification. Solvents were obtained from commercial sources and thoroughly deoxygenated prior to use. [ReOBr₃(dppe)] was prepared according to the literature [35].

Gaseous NO obtained in the reaction:



was purified by passing through the washers with concentrated KOH solution and over solid NaOH.

The reactions were performed under argon atmosphere.

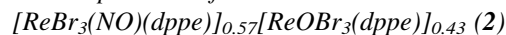
2.1. Preparation of [ReBr₃(MeCN)(dppe)] (**1**)

Triphenylphosphine (5 g, 19 mmol) was added to a suspension of [ReOBr₃(dppe)] (1 g, 1.2 mmol) in tetrahydrofuran (50 cm³) and acetonitrile (50 cm³). The brownish-orange solution thus formed was refluxed for 4 h. The volume was condensed to 15 cm³ and upon slow cooling to room temperature brownish-orange microcrystalline solid was isolated. X-ray quality crystals were obtained by recrystallization from acetonitrile. Yield 70%. The crystals of **1** are air stable in the solid state and in the acetonitrile solution but they slowly decompose with loss of acetonitrile in halogenated solvents such as chloroform and dichloromethane. A solution of **1** in CH₂Cl₂ and CHCl₃ can be stabilized by the addition of acetonitrile.

IR (KBr, cm⁻¹) 3053 (w), 2915 (w), 1484 (m), 1434 (s), 1418 (m), 1361 (w) 1332 (w), 1189 (w), 1157 (w), 1100 (s), 1027 (w), 998 (w) 870 (w), 815 (w), 752 (m), 741 (s), 697 (s), 653 (m), 522 (s), 501 (m), 458 (m).

Anal. Found: C, 38.92; H, 3.18; N, 1.68. Calc. for C₂₈H₂₇Br₃NP₂Re (**1**): C, 38.86; H, 3.14; N, 1.62.

2.2. Preparation of



NO was passing through a vigorously stirred and refluxing solution of [ReBr₃(MeCN)(dppe)] (1 g, 1.2 mmol) in toluene (50 cm³) for 4 h. The colour changed gradually from brownish-orange to dark red. Then the resulting solution was evaporated to the volume of 10 cm³. The dark red crystalline precipitate of **2** was formed by an addition of 40 cm³ of EtOH and after 15 min it was filtered off. The product was washed with cold ether and dried in vacuo. Yield 60%.

IR (KBr, cm⁻¹) 3052 (w), 2948 (w), 2910 (w) 1740 (vs) 1485 (m), 1435 (s), 1154 (w), 1128 (m), 1097 (s) 1027 (w), 998 (w), 970 (s), 820 (m), 740 (m), 725 (m), 689 (s), 655 (m), 546 (m), 521 (s), 495 (m), 444.

Anal. Found: C, 36.72; H, 2.73; N, 0.97. Calc. for C₂₆H₂₄P₂Br₃ON_{0.5}Re (**2**): C, 36.85; H, 2.85; N, 0.83.

2.3. Physical measurements

UV–vis spectra were recorded on a spectrophotometer Lab Alliance UV–vis 8500 in the range 800–220 nm in deoxygenated dichloromethane solution. IR spectra were recorded as KBr pellets with a Nicolet Magna 560 spectrophotometer in the spectral range 4000–400 cm⁻¹. The magnetic susceptibility was determined with a superconducting quantum interference device (SQUID, Quantum Design) magnetometer. Elemental analyses (CHN) were performed on a Perkin-Elmer CHN-2400 analyzer.

2.4. Crystal structures determination and refinement

The crystals of **1** and **2** suitable for X-ray structure determination were obtained by slow evaporation from acetonitrile. The X-ray intensity data were collected on KM-4-CCD automatic diffractometer equipped with CCD detector with ω scan mode, 30 and 42 s exposure time was used for **1** and **2**, respectively and, respectively all and a quarter of Ewald sphere up to 50.2° was collected. The unit cell parameters were determined from least-squares refinement of the setting angles of 8022 and 3139 of strongest reflections for **1** and **2** respectively. Details concerning crystal data and refinement are given in Table 1. Lorentz, polarization and numerical absorption corrections [36] were applied. The structures were solved direct methods and subsequently completed by the difference Fourier recycling. All the non-hydrogen atoms were refined anisotropically using full-matrix, least-squares technique. For compound **2** some restraints were applied, for details see Section 3 and 4. All hydrogen atoms were founded on difference Fourier synthesis

Table 1
Crystal data and structure refinement for **1** and **2**

	1	2
Empirical formula	C ₂₈ H ₂₇ Br ₃ NP ₂ Re	C ₂₆ H ₂₄ Br ₃ N ₀ 57OP ₂ Re
Formula weight	865.38	848.31
Temperature (K)	293(2)	291(2)
Wavelength (Å)	0.71073	0.71073
Crystal system	Monoclinic	Monoclinic
Space group	P2 ₁ /n	P2 ₁ /n
Unit cell dimensions	<i>a</i> = 9.7848(4) Å <i>b</i> = 22.5565(9) Å <i>c</i> = 13.8442(5) Å β = 102.404(3)°	<i>a</i> = 11.8735(8) Å <i>b</i> = 14.3697(11) Å <i>c</i> = 16.4129(9) Å β = 93.389(5)°
Volume (Å ³)	2984.2(2)	2795.4(3)
Z	4	4
Density (calculated, Mg/m ³)	1.926	2.016
Absorption coefficient (mm ⁻¹)	8.270	8.768
<i>F</i> (000)	1648	1608
Crystal size (mm)	0.54 × 0.13 × 0.06	0.36 × 0.07 × 0.01
θ range for data collection	2.95–25.11°	3.26–25.10°
Index ranges	–11 ≤ <i>h</i> ≤ 9 –26 ≤ <i>k</i> ≤ 26 –16 ≤ <i>l</i> ≤ 16	–14 ≤ <i>h</i> ≤ 14 0 ≤ <i>k</i> ≤ 17 0 ≤ <i>l</i> ≤ 19
Reflections collected	30,654	4970
Independent reflections	5321 (<i>R</i> _{int} = 0.0439)	4970 (<i>R</i> _{int} = 0.0000)
Completeness to 2 θ (%)	97.1	95.6
Max. and min. transmission	0.6562 and 0.0949	0.894 and 0.144
Data/restraints/parameters	5321/0/317	4970/33/317
Goodness-of-fit on <i>F</i> ²	1.056	1.006
Final <i>R</i> indices [<i>I</i> > 2 σ (<i>I</i>)]	<i>R</i> 1 = 0.0291 <i>wR</i> 2 = 0.0567	<i>R</i> 1 = 0.0526 <i>wR</i> 2 = 0.1017
<i>R</i> indices (all data)	<i>R</i> 1 = 0.0433 <i>wR</i> 2 = 0.0610	<i>R</i> 1 = 0.0951 <i>wR</i> 2 = 0.1216
Largest diff. peak and hole (e Å ⁻³)	1.444 and –0.660	1.458 and –1.196

and refined as ‘riding’ on their parent carbon atoms with geometry idealisation after each cycle and assigned isotropic temperature factors equal 1.2 times the value of equivalent temperature factor of the parent non methyl carbon atoms and 1.5 for methyl carbon atoms. SHELXS97 [37], SHELXL97 [38] and SHELXTL [39] programs were used for all the calculations. Atomic scattering factors were those incorporated in the computer programs.

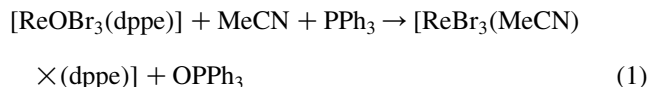
2.5. Computational details

GAUSSIAN03 program [40] was used in the calculations. The geometry optimization of [ReBr₃(NO)(dppe)] and [ReOBr₃(dppe)] was carried out with the DFT method with the use of B3LYP functional [41,42]. The spin-allowed transitions with the TDDFT method [43] were calculated for [ReOBr₃(dppe)] and [Re(NO)Br₃(dppe)]. LANL2DZ basis set [44] was used on the rhenium atom, 6-31G(d) on the bromine, nitrogen and carbon atoms and 6-31G basis on the hydrogen atoms in the calculations.

3. Results and discussion

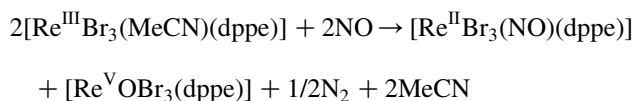
3.1. Preparation of complexes

The nitrile complex **1** has been prepared in high yield by use of the procedure shown in Eq. (1).



It can be assumed that the [ReBr₃(dppe)] compound, generated from [ReOBr₃(dppe)] and PPh₃ in the first step of the synthesis, reacts with MeCN to give **1**. The mass ratio of [ReOBr₃(dppe)] and PPh₃ equal to 1:5 ensures the maximum yield of the product. In the case of smaller excess of PPh₃, some unreacted starting material has been recovered from the reaction.

Complex **1** reacts easily with gaseous nitric oxide to give the mixed [ReBr₃(NO)(dppe)]_{0.57}[ReOBr₃(dppe)]_{0.43} complex (**2**) with rhenium atoms on +2 and +5 oxidation states. The reaction equation:



explains the formation of complex **2**.

3.2. Description of the crystal structure of **1**

Compound **1** crystallises in the monoclinic space group P2₁/n and its structure consists of discrete and well-separated monomers linked *via* C(2)–H(2A)⋯Br(2)(*x* + 1/2, –*y* + 3/2, *z* + 1/2) [D⋯A distance equals 3.858(5) Å and D–H⋯A angle 170.3°], C(32)–H(32A)⋯Br(1)(–*x*, –*y* + 2, –*z*) [D⋯A distance equals 3.513(6) Å and D–H⋯A angle 135.8°] and C(32)–H(32B)⋯Br(3)(–*x* + 1, –*y* + 2, –*z*) [D⋯A distance equals 3.624(6) Å and D–H⋯A angle 149.6°] intermolecular weak hydrogen bonds [45]. The conformations of molecules of compound **1** are stabilised by weak intramolecular hydrogen bond: C(16)–H(16)⋯Br(2) [D⋯A distance equals 3.732(5) Å and D–H⋯A angle 151.6°]. The molecular structure of **1** is presented in Fig. 1.

The rhenium atom is in a distorted octahedral environment with terminal MeCN group [Re–N–C angle—176.0(4)°] *trans* to one of the phosphorus atoms of the chelate ligand—bis(diphenylphosphino)ethane and three bromine ligands in meridional geometry.

The most important bond lengths and angles for **1** are reported in Table 2.

The Re–N(nitrile) bond length of 2.127(4) Å in **1** agrees well with the Re–N values found in the rhenium complexes containing the nitrile ligand in *trans* position to a strong π -acceptor, but it is significantly longer than the Re–N bond lengths found for the complexes whose *trans* position to the nitrile ligand is not occupied by a π -acceptor.

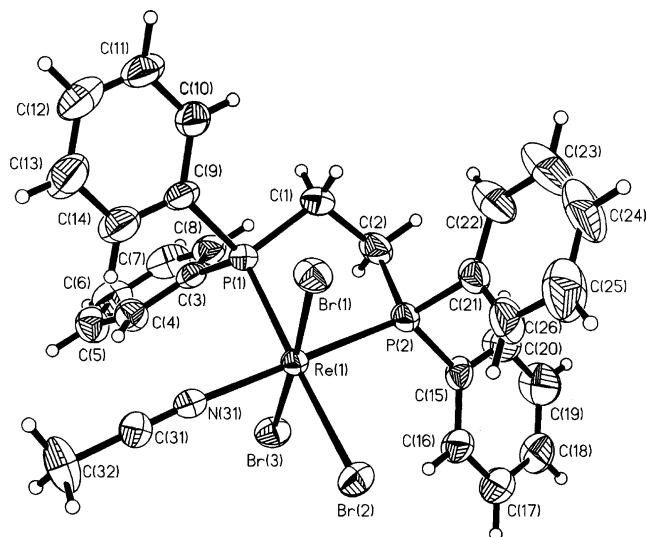


Fig. 1. The molecular structure of **1**. The thermal ellipsoids are drawn at 50% probability level.

In $[\text{ReBr}_3(\text{NO})(\text{MeCN})(\text{PPh}_3)]$ [13] and $[\text{NEt}_4][\text{ReBr}_4(\text{NO})(\text{MeCN})]$ [46] with acetonitrile *trans* to nitrosyl group the Re–N(nitrile) bond lengths are equal to 2.156(7) and 2.153(11) Å, respectively, but for *mer-trans*- $[\text{ReCl}_3(\text{MeCN})(\text{PPh}_3)_2]$ the Re–N distance is 2.068(5) Å [47].

A clear *trans* effect of dppe ligand is also observed in the elongation of Re–Br(2) distance *trans* to the phosphorus atom of the dppe ligand [2.5980(5) Å], the mutually *trans*

Table 2

Table 2 The experimental bond lengths (Å) and angles (°) for **1**

Bond lengths	Experimental
Re(1)–N(31)	2.127(4)
Re(1)–P(1)	2.3991(13)
Re(1)–P(2)	2.4021(12)
Re(1)–Br(1)	2.4801(5)
Re(1)–Br(2)	2.5980(5)
Re(1)–Br(3)	2.4736(5)
N(31)–C(31)	1.098(5)
C(31)–C(32)	1.463(7)
Angles	
N(31)–Re(1)–P(1)	95.56(10)
N(31)–Re(1)–P(2)	178.58(11)
P(1)–Re(1)–P(2)	83.50(4)
N(31)–Re(1)–Br(1)	90.63(10)
N(31)–Re(1)–Br(2)	84.42(10)
N(31)–Re(1)–Br(3)	88.96(10)
P(1)–Re(1)–Br(1)	84.80(3)
P(1)–Re(1)–Br(2)	176.77(3)
P(1)–Re(1)–Br(3)	90.95(3)
P(2)–Re(1)–Br(1)	90.35(3)
P(2)–Re(1)–Br(2)	96.58(3)
P(2)–Re(1)–Br(3)	89.99(3)
Br(1)–Re(1)–Br(2)	91.971(18)
Br(3)–Re(1)–Br(1)	175.666(19)
Br(3)–Re(1)–Br(2)	92.282(18)
C(31)–N(31)–Re(1)	176.0(4)
N(31)–C(31)–C(32)	178.4(5)

Re–Br bonds are equal to 2.4801(5) and 2.4736(5) Å, respectively. The Re–P distances at 2.3991(13) and 2.4021(12) Å in **1** are shorter than those found in the rhenium complexes with chelate phosphine ligands: 2.450(4), 2.456(4) and 2.480(4) Å in *mer*- $[\text{ReCl}_3(\text{dppm-P,P}')(\text{dppom-P})]$ [48] and 2.479(1) and 2.458(2) Å in *trans*- $[\text{ReCl}(\text{NO})(\text{dppe})_2]^{2+}$ [49]. The bond valences were computed as $\nu_{ij} = \exp[(R_{ij} - d_{ij})/B]$ [50–52], where R_{ij} is the bond-valence parameter (in the formal sense R_{ij} is the single-bond length between i and j atoms) [53]. The $R_{\text{Re-N}}$, $R_{\text{Re-P}}$, $R_{\text{Re-O}}$, $R_{\text{Re-Br}}$ were taken as 2.06, 2.46, 1.97 and 2.45 [50], respectively, and the value of B was taken as 0.37 [51]. The computed bond valences of the rhenium atom are $\nu_{\text{Re-N}} = 0.834$, $\nu_{\text{Re-P}} = 1.169$ and 1.179, $\nu_{\text{Re-Br}} = 0.607$, 0.922 and 0.938 v.u. (valence units), what means that dppe ligand is the strongest bonded substituent, two bromide atoms and nitrile substituent is bonded with comparable strength, and one bromide atom is bonded distinctly weaker. The significant shortening of the C–N bond length in **1** [1.098(5) Å] in comparison with free acetonitrile [1.155 Å] [54] is observed and it is expected upon coordination. The NC–CH₃ distance is within the range observed for other acetonitrile complexes [13,46,47].

3.3. Description of the crystal structure of **2**

The results of the structural study on **2** show clearly that the molecules of $[\text{ReBr}_3(\text{NO})(\text{dppe})]$ are packed together with molecules of $[\text{ReOBr}_3(\text{dppe})]$ in a not unambiguous proportion. Depending on the scheme of disordered substituents restraining it differs from 57:43 to 50:50. The molecules of **2** are linked *via* C(20)–H(20)⋯Br(1) ($-x + 3/2$, $y - 1/2$, $-z + 1/2$) [D⋯A distance equals 3.642(14) Å and D–H⋯A angle 149.1°] intermolecular weak hydrogen bonds [45]. The numbering scheme of the disordered complex **2** is shown in Fig. 2.

In the both molecules the rhenium atom has a distorted octahedral coordination with the chelate phosphine ligand

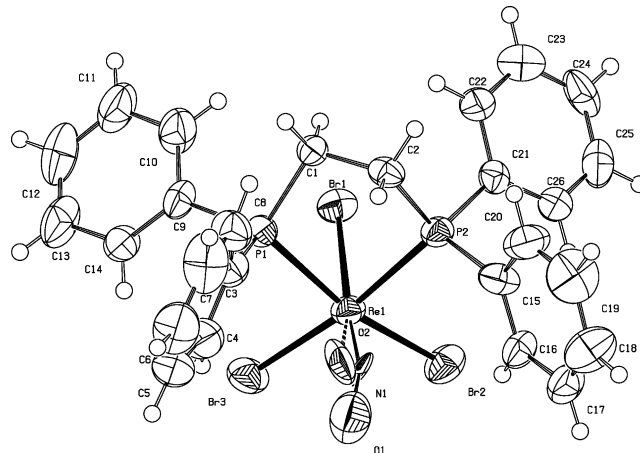


Fig. 2. The molecular structure of **2**.

Table 3

The experimental bond lengths (Å) and angles (°) for **2** and [ReOBr₃(dppe)] and the optimized bond lengths (Å) and angles (°) for [Re(NO)Br₃(dppe)] and [ReOBr₃(dppe)]. The experimental bond lengths (Å) and angles (°) for [ReOBr₃(dppe)] are taken from the paper [64]

Bond lengths	2 Experimental (this work)	[ReOBr ₃ (dppe)] Experimental [64]	[Re(NO)Br ₃ (dppe)] Optimized	[ReOBr ₃ (dppe)] Optimized
Re(1)–O(2)	1.72(3)	1.680		1.687
Re(1)–N(1)	1.679(15)		1.764	
Re(1)–P(1)	2.463(3)	2.447	2.507	2.505
Re(1)–P(2)	2.461(3)	2.463	2.510	2.513
Re(1)–Br(1)	2.5759(12)	2.581	2.667	2.703
Re(1)–Br(2)	2.5192(13)	2.517	2.621	2.618
Re(1)–Br(3)	2.5316(13)	2.517	2.619	2.613
N(1)–O(1)	1.18(2)		1.177	
<i>Angles</i>				
O(2)–Re(1)–P(1)	83.1(13)	83.3		84.8
N(1)–Re(1)–P(1)	96.8(9)		95.52	
O(2)–Re(1)–P(2)	90.6(14)	91.2		89.9
N(1)–Re(1)–P(2)	87.7(12)		93.06	
P(1)–Re(1)–P(2)	82.49(10)	83.2	82.56	84.5
O(2)–Re(1)–Br(2)	109.1(13)	104.4		102.9
N(1)–Re(1)–Br(2)	95.0(9)		92.40	
P(2)–Re(1)–Br(2)	91.45(8)	96.0	89.54	93.1
P(1)–Re(1)–Br(2)	166.46(8)	164.3	169.09	166.7
O(2)–Re(1)–Br(3)	94.3(13)	100.7		102.9
N(1)–Re(1)–Br(3)	98.5(11)		91.89	
P(2)–Re(1)–Br(3)	172.35(7)	174.6	168.84	172.6
P(1)–Re(1)–Br(3)	92.25(8)	93.1	87.01	92.6
Br(2)–Re(1)–Br(3)	92.50(5)	86.5	100.24	88.2
O(2)–Re(1)–Br(1)	162.2(14)	162.6		162.7
N(1)–Re(1)–Br(1)	171.8(12)		178.62	
P(2)–Re(1)–Br(1)	84.64(7)	82.6	85.63	82.3
P(1)–Re(1)–Br(1)	79.26(7)	76.9	83.86	77.6
Br(2)–Re(1)–Br(1)	88.16(4)	87.4	88.06	89.2
Br(3)–Re(1)–Br(1)	88.93(4)	92.8	89.31	90.5
O(1)–N(1)–Re(1)	162(3)		179.33	

and two bromide ions in the equatorial plane. The axial positions of the molecules are occupied by the NO group or oxo ligand and bromide Br(1) ion. The clear distortions from octahedral symmetry of the Re center in **2** are induced by the nitrosyl/oxo compositional disorder, the presence of bidentate (dppe) and multiply bonding (oxo, nitrosyl) ligands. Significant deviations from linearity are observed in O(2)–Re(1)–Br(1) [162.2(14)°] and P(1)–Re(1)–Br(2) [166.46(8)°]. The bond angles between *cis*-ligands vary between 82.49(10) and 109.1(13)°. The most important bond lengths and angles for **2** are reported in Table 3.

For compound **2**, due to the nitrosyl/oxo compositional disorder, in the no restrained refinement can be observed the elongation of Re–NO distance [1.92(4) Å] and the shortening of N–O bond length [1.03(4) Å] in comparison with other rhenium nitrosyl complexes. In monoclinic polymorph of *mer-cis*-[ReBr₃(NO)(OPPh₃)₂] the Re–NO bond length is 1.757(12) Å and N–O distance is 1.261(13) Å [18] and in [ReBr₄(NO)(EtOH)][−] the Re–NO bond length is 1.723(15) and N–O distance is 1.19(2) Å [46]. As a consequence of disorder in not restrained refinement the shortening of

the Re–O(2) distance [1.607(18) Å] in comparison with other Re(V) monooxocomplexes: 1.669(4) Å in [ReOCl₃(PPh₃)(OPPh₃)] [55] and 1.671(6) Å in *fac*-[ReOCl₃(dppm-P,P′)] (dppm = Ph₂PCH₂PPh₂) [56] is observed. The fact that disorder cause violations in determined distances is also confirmed by calculated bond valences, which are $\nu_{\text{Re-N}} = 1.460$, $\nu_{\text{Re-O}} = 2.667$ v.u. According to valence sum rule [52] these values should be almost the same in correctly refined disordered structures. Thus as the best one was selected refinement with Re–N, N–O and Re–O distances fixed and NO, O substituents restrained with effective standard deviation 0.04 to have the same U_{ij} components (after approximating to isotropic behaviour). The Re(1)–Br(1) distance, considerable longer than Re(1)–Br(2) and Re(1)–Br(3) bond lengths, is determined by the presence of oxygen atom or nitrosyl group in *trans* position. The structural *trans* effect of oxo and nitrosyl ligands was observed in many transition metal complexes [57]. According to the computed bond valences ($\nu_{\text{Re-P}} = 0.997$ and 0.992 , $\nu_{\text{Re-Br}} = 0.711$, 0.829 and 0.802 v.u) it can be stated that dppe ligand is bonded distinctly weaker than in compound **1**, and the Re–P bonds are only slightly stronger than Re–Br bonds.

Table 4

The possible oxidation numbers and spin multiplicities of Re and NO in [ReBr₃(NO)(dppe)]

Re	Spin of Re	NO	Spin of NO	Total spin	Spin multiplicity
Re(II)	5/2, 3/2, 1/2	NO ⁺ (π_1^*) ⁰ (π_2^*) ⁰	0	5/2, 3/2, 1/2	6, 4, 2
Re(III)	2, 1, 0	NO (π_1^*) ¹ (π_2^*) ⁰	1/2	5/2, 3/2, 1/2	6, 4, 2
Re(IV)	3/2, 1/2	NO ⁻ (π_1^*) ¹ (π_2^*) ¹	1	5/2, 3/2, 1/2	6, 4, 2

3.4. Spectroscopic characterization and magnetochemical measurements

The IR spectra of **1** and **2** are governed by the vibrations of the phosphine ligand. The $\nu(\text{C}\equiv\text{N})$ vibration is absent in **1**, as already noted for other monomeric rhenium(III) nitrile complexes [58–60]. However, the absence of the characteristic strong $\nu(\text{Re}=\text{O})$ band at $\sim 970\text{ cm}^{-1}$ is a clear indication that there is no oxo-Re(V) starting material left in the sample **1**. The IR spectrum of **2** exhibits strong band at 970 cm^{-1} assignable to $\nu(\text{Re}=\text{O})$ mode and strong band at 1740 cm^{-1} corresponding to $\nu(\text{NO})$. The value of $\nu(\text{NO})$ corresponds to linear NO range of Haymore and Ibers [$\nu(\text{NO})$ above $1620\text{--}1610\text{ cm}^{-1}$ were assigned to linear M–N–O systems, while $\nu(\text{NO})$ below 1610 cm^{-1} were assigned to bent M–N–O systems] [61].

Table 5

The energy and character of upper valence molecular orbitals for [ReBr₃(NO)(dppe)] and [ReOBr₃(dppe)]

MO	[Re(NO)Br ₃ (dppe)]			[ReOBr ₃ (dppe)]		
	α	Character	β	Character	Character	
HOMO-12	-7.465	$\pi(\text{Ph})$	-7.481	$\pi(\text{Ph}), n(\text{P})$	-7.479	$\pi(\text{Ph})$
HOMO-11	-7.444	$\pi(\text{Ph}), n(\text{P})$	-7.465	$\pi(\text{Ph})$	-7.364	$\pi(\text{Ph})$
HOMO-10	-7.345	$\pi(\text{Ph})$	-7.388	$\pi(\text{Ph}), n(\text{P})$	-7.285	$\pi(\text{Ph})$
HOMO-9	-7.180	$\pi(\text{Ph})$	-7.327	$\pi(\text{Ph})$	-7.221	$\pi(\text{Ph})$
HOMO-8	-7.111	$\pi(\text{Ph})$	-7.153	$\pi(\text{Ph})$	-7.169	$\pi(\text{Ph})$
HOMO-7	-7.057	$\pi(\text{Ph}), n(\text{P})$	-7.096	$\pi(\text{Ph})$	-7.087	$\pi(\text{Ph})$
HOMO-6	-6.981	$\pi(\text{Ph}), n(\text{P})$	-7.036	$\pi(\text{Ph}), n(\text{P})$	-6.999	$\pi(\text{Ph}), n(\text{P})$
HOMO-5	-6.611	$\pi(\text{Br})$	-6.956	$\pi(\text{Ph}), n(\text{P})$	-6.779	$\pi(\text{Br}), \pi(\text{O}), n(\text{P})$
HOMO-4	-6.306	$d_{xz} + \pi^*(\text{NO}); \pi(\text{Br})$	-6.262	$\pi(\text{Br})$	-6.670	$\pi(\text{Br}), \pi(\text{O}), n(\text{P})$
HOMO-3	-6.250	$d_{yz} + \pi^*(\text{NO}); \pi(\text{Br})$	-6.224	$d_{xz} + \pi^*(\text{NO}); \pi(\text{Br})$	-6.366	$\pi(\text{Br})$
HOMO-2	-6.119	$\pi(\text{Br})$	-6.167	$d_{yz} + \pi^*(\text{NO}); \pi(\text{Br})$	-6.240	$\pi(\text{Br})$
HOMO-1	-6.020	$\pi(\text{Br})$	-6.094	$\pi(\text{Br})$	-6.099	$\pi(\text{Br})$
HOMO	-5.872	$d_{xy} + \sigma^*(\text{P}) - \pi(\text{Br})$	-6.008	$\pi(\text{Br})$	-5.765	$d_{xy} - \pi(\text{Br})$
LUMO	-1.603	$d_{x^2-y^2} - \sigma(\text{Br}) - \sigma(\text{P}), \pi^*(\text{NO})$	-3.673	$d_{xy} + \sigma^*(\text{P}) - \pi(\text{Br})$	-2.991	$d_{xz} - \pi(\text{O})$
LUMO+1	-1.551	$\pi^*(\text{NO}) - d_{xz}$	-1.560	$\pi^*(\text{NO}) - d_{xz}$	-2.868	$d_{yz} - \pi(\text{O})$
LUMO+2	-1.439	$\pi^*(\text{NO}) - d_{yz}$	-1.521	$\pi^*(\text{NO}) - d_{yz}$	-1.549	$d_{x^2-y^2} - \sigma(\text{Br}) - \sigma(\text{P})$
LUMO+3	-1.208	$p_x(\text{P}) + \pi^*(\text{Ph})$	-1.379	$d_{x^2-y^2} - \sigma(\text{Br}) - \sigma(\text{P}), \pi^*(\text{NO})$	-1.168	$p_x(\text{P}) + \pi^*(\text{Ph})$
LUMO+4	-1.180	$p_y(\text{P}) + \pi^*(\text{Ph}), d_{z^2} - \sigma(\text{Br}) - \sigma(\text{N})$	-1.167	$p_x(\text{P}) + \pi^*(\text{Ph})$	-1.161	$p_y(\text{P}) + \pi^*(\text{Ph})$
LUMO+5	-1.104	$\sigma^*(\text{P}-\text{Ph})$	-1.112	$p_y(\text{P}) + \pi^*(\text{Ph})$	-1.042	$\sigma^*(\text{P}-\text{Ph}), d_z^2 - \sigma(\text{Br}) - \sigma(\text{O})$
LUMO+6	-0.703	$\pi^*(\text{Ph})$	-1.056	$\sigma^*(\text{P}-\text{Ph}), d_z^2 - \sigma(\text{Br}) - \sigma(\text{N})$	-0.548	$\pi^*(\text{Ph})$
LUMO+7	-0.538	$\pi^*(\text{Ph})$	-0.695	$\pi^*(\text{Ph})$	-0.499	$\pi^*(\text{Ph})$
LUMO+8	-0.390	$\pi^*(\text{Ph})$	-0.528	$\pi^*(\text{Ph})$	-0.464	$\pi^*(\text{Ph})$
LUMO+9	-0.318	$\pi^*(\text{Ph})$	-0.368	$\pi^*(\text{Ph})$	-0.360	$\pi^*(\text{Ph})$
LUMO+10	-0.206	$\pi^*(\text{Ph}), d_{x^2-y^2} - \sigma(\text{Br}) - \sigma(\text{P})$	-0.305	$\pi^*(\text{Ph})$	-0.293	$\pi^*(\text{Ph})$
LUMO+11	-0.169	$d_{z^2} - \sigma(\text{Br}) - \sigma(\text{N})$	-0.143	$d_{x^2-y^2} - \sigma(\text{Br}) - \sigma(\text{P}), \pi^*(\text{Ph})$	0.072	$d_{z^2} - \sigma(\text{Br}) - \sigma(\text{O})$

The complex **1** shows room temperature magnetic moments of 1.43 BM. This value is characteristic of the mononuclear complexes with low-spin rhenium(III) (d^4) ions in O_h field [62], and arises because of the large spin-orbit coupling ($\xi = 2500\text{ cm}^{-1}$) [63]. Due to the large spin-orbit coupling, the recording of X-band ESR spectra of solutions of these complexes is impossible even at 100 K.

3.5. Geometry and electronic structure

The geometries of [ReOBr₃(dppe)] and [ReBr₃(NO)(dppe)] were optimized with the DFT method in singlet and doublet state, respectively. Table 4 shows the possible electronic configurations and spin multiplicities of the [ReBr₃(NO)(dppe)] complex. Doublet state agrees well with the magnetic measurements for **2**. The most important

optimized bond lengths and angles for the $[\text{ReOBr}_3(\text{dppe})]$ and $[\text{ReBr}_3(\text{NO})(\text{dppe})]$ are reported in Table 3. For $[\text{ReOBr}_3(\text{dppe})]$ there is a good accordance of the experimental data [64] with the calculated bond lengths and angles. Some differences between the experimental and calculated data can be noticed for the nitrosyl complex. However, the disagreement results mainly from the nitrosyl/oxo compositional disorder in **2**. High electronic density along the Re–O axis in $[\text{ReOBr}_3(\text{dppe})]$ strongly influences the positions of the adjacent bromine atoms, which are pushed away. This feature causes a strong deviation from linearity of the O–Re–Br(1) sequence. The elongation of Re–Br(1) in comparison with Re(1)–Br(2) and Re(1)–Br(3) bond lengths, determined by the presence of the oxygen atom or nitrosyl group in *trans* position, is reproduced in the optimized structures.

The energies and characters of the several HOMO and LUMO orbitals of $[\text{ReBr}_3(\text{NO})(\text{dppe})]$ and $[\text{ReOBr}_3(\text{dppe})]$ are presented in Table 5. The selected HOMO and LUMO orbitals of the nitrosyl complex with α spin are depicted in Fig. 3. The *z* axis goes along the Br(1)–Re–N(1) linkage and Br(1)–Re–O(2) in $[\text{ReBr}_3(\text{NO})(\text{dppe})]$ and $[\text{ReOBr}_3(\text{dppe})]$, respectively. Due to the presence of dppe in the coordination sphere, most of the MOs have complicated character.

The bonding of NO to the rhenium centre involves a synergic interaction between the NO ligand orbitals and the metal orbitals. The Re–NO bond consists of two components: (i) a donation of electron density from a σ -type orbital on NO onto the metal orbital and (ii) a donation of electron density from the occupied metal d-orbitals into the π^* antibonding orbitals of NO ligand. The HOMO-1, HOMO-3 with α -spin and HOMO-3, HOMO-2 with β -spin

present the π -bonding interaction between d_{yz} and d_{xz} metal orbitals and π^* NO orbitals. However, the structure of these orbitals is a little more complicated—in all them the lone pair orbitals of bromine with π character have contribution. The LUMO+1, LUMO+2 with α -spin and LUMO+1, LUMO+2 with β -spin are of the $\pi_{\text{Re–NO}}^*$ antibonding character.

The d_{xy} rhenium orbital and π orbitals of bromine ligands in anti-bonding arrangement make main contributions into the HOMO with α -spin and LUMO with β -spin. The HOMO with β -spin is localised on the bromine ligand in *trans* position to NO group.

The LUMO with α -spin and LUMO+3 with β -spin are of $d_{x^2-y^2}-\sigma_{\text{Br}}-\sigma_{\text{P}}$ character with the contribution of π_{NO}^* .

The selected HOMO and LUMO orbitals of the oxo complex are depicted in Fig. 4.

The rhenium–oxygen interaction in $[\text{ReOBr}_3(\text{dppe})]$ is described as a triple bond. The π bonds arise from overlap of the two occupied oxygen p_π orbitals with the empty d_{xz} and d_{yz} metal orbitals. The HOMO-34 and HOMO-33 of $[\text{ReOBr}_3(\text{dppe})]$ are of $\pi_{\text{Re=O}}$ bonding character, whereas the LUMO and LUMO+1 are ascribed as π -antibonding rhenium–oxygen molecular orbitals. The HOMO is formed by antibonding interaction between d_{xy} rhenium orbital and the lone pair orbitals of two bromine ligands with π character.

3.6. Electronic spectra

The electronic spectra of $[\text{ReOBr}_3(\text{dppe})]$ and **2** are presented in Fig. 5. The calculated electronic transitions of $[\text{ReOBr}_3(\text{dppe})]$ and $[\text{ReBr}_3(\text{NO})(\text{dppe})]$ and the experimental absorption bands of the oxo-complex are gathered

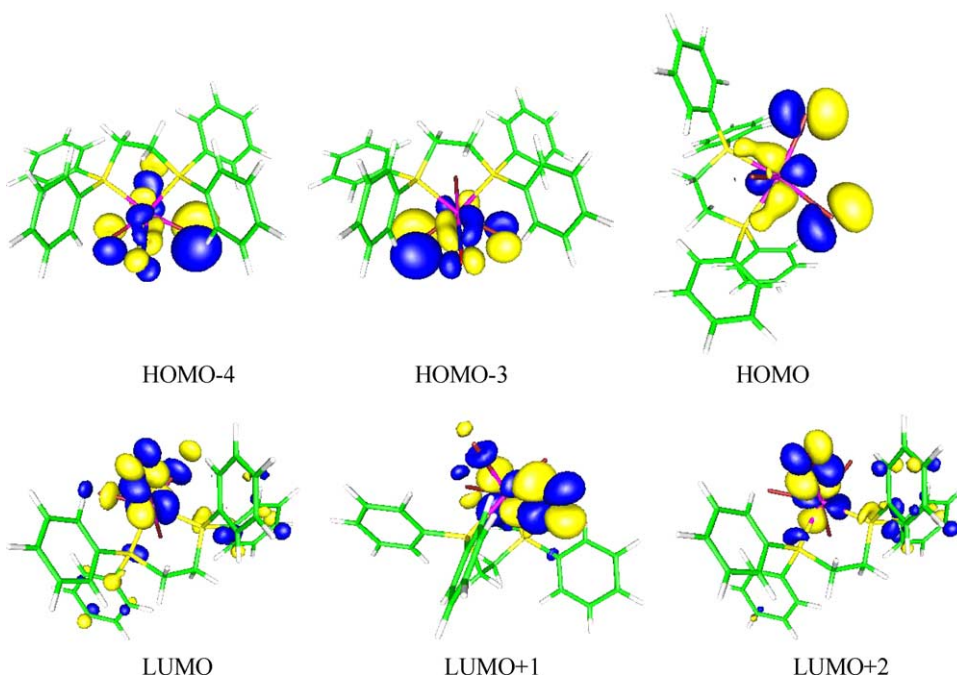


Fig. 3. The selected HOMO and LUMO orbitals with α -spin for $[\text{ReBr}_3(\text{NO})(\text{dppe})]$.

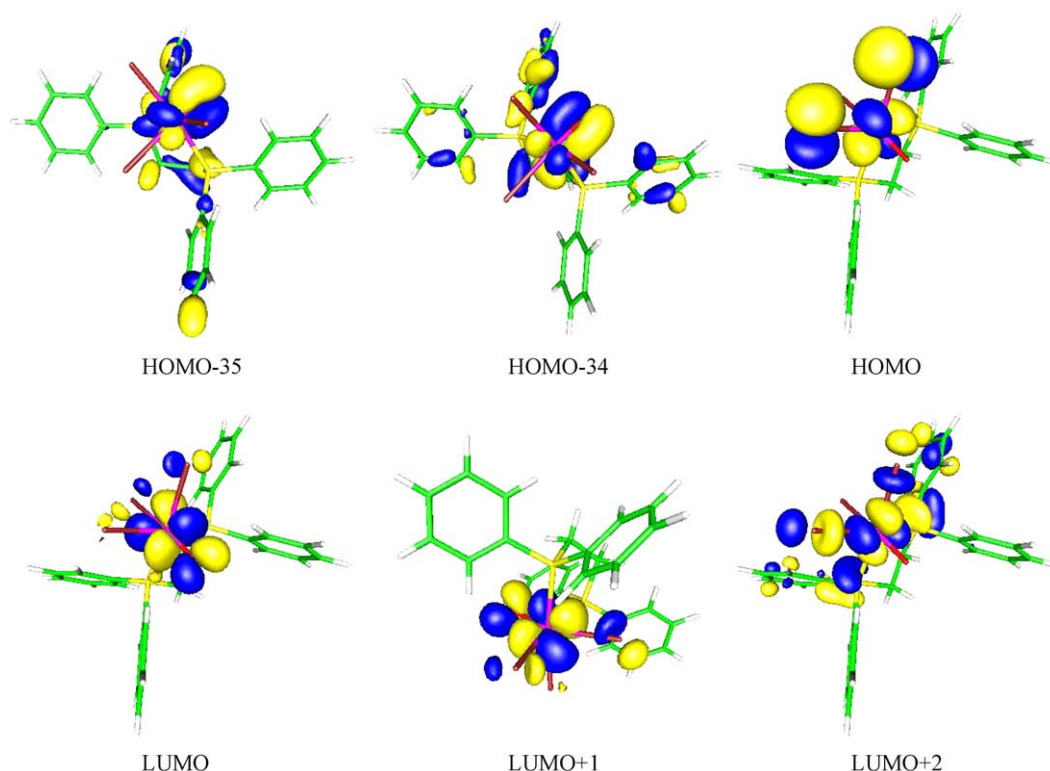


Fig. 4. The selected HOMO and LUMO orbitals for $[\text{ReOBr}_3(\text{dppe})]$.

in Tables 6 and 7, respectively. Except for the low energy part of the spectra, only transitions with oscillator strengths larger than 0.01 are listed. The assignment of the calculated transitions to the experimental bands was based on the criterion of the energy and oscillator strengths of the calculated transitions. The longest wavelength experimental bands are of low intensity and they are compared to the calculated long-wave transitions with small oscillator strengths. The remaining absorption experimental bands are of much higher intensity and they are compared to the calculated transitions with high oscillator strengths.

The longest wavelength experimental bands of $[\text{ReOBr}_3(\text{dppe})]$ at 640 and 535 nm may be attributed to the calculated transitions of $d \rightarrow d$ character at 776.4 and 406.5 nm, respectively. The calculated at 453.5 nm electronic transition of $\pi_{\text{Br}} \rightarrow d$ origin makes contribution into the second of them. Basing on the CFT theory, three spin-allowed singlet–singlet $d \rightarrow d$ transitions may be predicted for d^2 configuration in O_h field: ${}^1A_1 \rightarrow {}^1E$, ${}^1A_1 \rightarrow {}^1A_2$ and ${}^1A_1 \rightarrow {}^1B_2$. The third $d \rightarrow d$ transition of $[\text{ReOBr}_3(\text{dppe})]$ was calculated at higher energy—at 250.7 nm.

The experimental band at 354 nm is very broad (Fig. 5) and it can be ascribed to the calculated transitions in the range 392–275 nm with $\pi(\text{Br})/\pi(\text{O})/n(\text{P}) \rightarrow d$ character (LMCT transitions). The most intense experimental band at 242.8 nm is attributed to the calculated transitions in the range 270–240 nm. These transitions are of LMCT ($\pi_{\text{Ph}} \rightarrow d$), MLCT ($d \rightarrow \pi_{\text{Ph}}^*$) and LLCT ($\pi_{\text{Br}} \rightarrow \pi_{\text{Ph}}^*$)

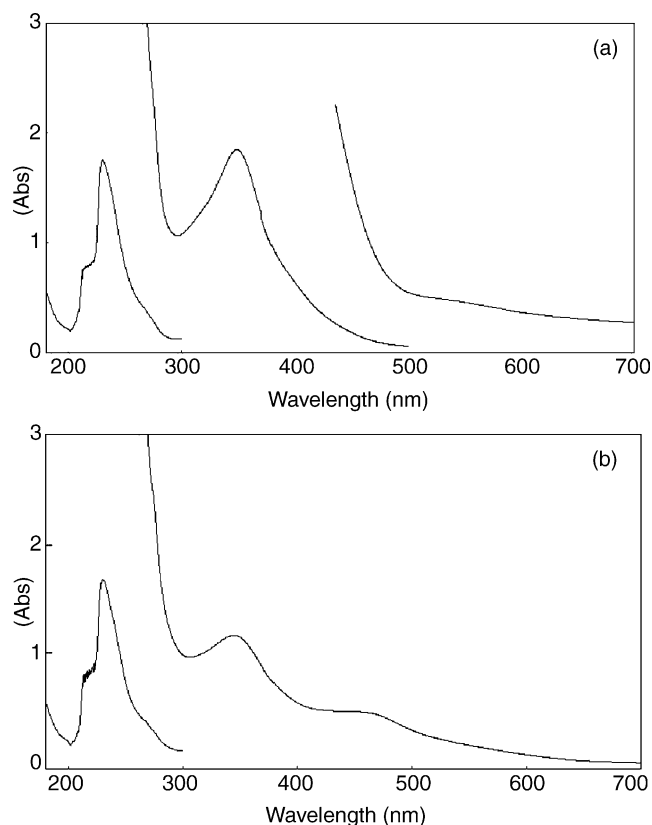


Fig. 5. The electronic absorption spectra of $[\text{ReOBr}_3(\text{dppe})]$ (a) and 2 (b).

Table 6

The energy and molar absorption coefficients of experimental absorption bands and the electronic transitions calculated with the TDDFT method for [ReOBr₃(dppe)]

The most important orbital excitations	Character	λ (nm)	E (eV)	f	Experimental A (nm) (E (eV)) _e
H→L+1	d→d	776.4	1.60	0.0001	640.0(1.94)30
H→3→L+1	π (Br)→d	453.8	2.73	0.0173	535.0(2.32)250
H→L+2	d→d	406.5	3.05	0.0301	
H→5→L	π (Br), π (O), n(P)→d	392.4	3.16	0.0383	354.0(3.50)8965
H→4→L+1	π (Br), π (O), n(P)→d				
H→15→L+1	π (Br)→d	299.3	4.14	0.0186	
H→17→L	σ (Br)→d	282.5	4.39	0.0175	
H→4→L+2	π (Br), π (O), n(P)→d				
H→5→L+2	π (Br), π (O), n(P)→d	279.8	4.43	0.0172	
H→5→L+2	π (Br), π (O), n(P)→d	277.6	4.47	0.0200	
H→2→L+3	π (Br)→ π^* (Ph)	276.6	4.48	0.0529	242.8(5.11)24185
H→2→L+5	π (Br)→ π^* (Ph))				
H→3→L+5	π (Br)→ π^* (Ph)	270.0	4.59	0.0104	
H→17→L+1	σ (Br)→d	267.8	4.63	0.0237	
H→L+7	d→ π^* (Ph)				
H→L+6	d→ π^* (Ph)	265.7	4.67	0.0102	
H→L+7	d→ π^* (Ph)				
H→6→L+2	π (Ph)→d	254.5	4.87	0.0117	
H→L+9	d→ π^* (Ph)				
H→7→L+2	π (Ph)→d	250.7	4.94	0.0265	
H→L+11	d→d				
H→4→L+3	π (Br), π (O), n(P)→ π^* (Ph)	249.9	4.96	0.0160	
H→8→L+2	π (Ph)→d	248.5	4.99	0.0381	
H→4→L+5	π (Br), π (O), n(P)→ π^* (Ph)				
H→1→L+6	π (Br)→ π^* (Ph)	247.9	5.00	0.0139	
H→1→L+7	π (Br)→ π^* (Ph)				

character. The transitions from metal to π_{ph}^* orbitals and from π_{ph} orbitals to metal are mediated by phosphorus orbitals, whereas the LLCT transitions ($\pi_{\text{Br}} \rightarrow \pi_{\text{ph}}^*$)—by phosphorus and rhenium orbitals.

The UV–vis spectrum of **2** exhibits four broad absorption bands at 559.3(1070), 457.6(2980), 352.8(5440) and 232.8 nm(42250) (Fig. 5). The lowest energy band of **2** at

559.3 nm can be assigned to the transition of d→d origin in [ReOBr₃(dppe)] and the transition of $\pi_{\text{Br}} \rightarrow \text{d}$ character (at 691.2 nm) in [Re(NO)Br₃(dppe)]. The second experimental band of **2** corresponds to d→ π_{NO}^* charge transfers transitions in [Re(NO)Br₃(dppe)], the oxocomplex does not show the absorption band in this range. The experimental bands of **2** at 457.6 and 352.8 nm are of

Table 7

The electronic transitions calculated with the TDDFT method for [ReBr₃(NO)(dppe)]

The most important α -spin orbital excitations	Character	The most important β -spin orbital excitations	Character	λ (nm)	E (eV)	f
H→4→L+1	$d_{xz} \rightarrow \pi_{\text{NO}}^*$	H-4→L	π (Br)→d	691.2	1.79	0.0291
H→3→L+2	$d_{yz} \rightarrow \pi_{\text{NO}}^*$	H→3→L+2	$d_{xz} \rightarrow \pi_{\text{NO}}^*$	520.3	2.38	0.0041
		H→5→L	π (Ph), n(P)→d	484.8	2.56	0.0047
		H→10→L	π (Ph), n(P)→d	462.6	2.68	0.0238
		H→9→L	π (Ph)→d			
H→L	d→d			424.9	2.92	0.0034
		H→13→L	π (Br)→d	417.5	2.97	0.0107
H→L	d→d	H→16→L	σ (Br)→d	405.6	3.06	0.0124
H→L+2	$d_{xy} \rightarrow \pi_{\text{NO}}^*$			382.4	3.24	0.0014
		H→18→L	σ (Br)→d	362.1	3.42	0.0054
		H→17→L	σ (Br)→d	357.8	3.47	0.0035
		H→1→L+1	π (Br)→ π_{NO}^*	318.5	3.89	0.0145
H→4→L+2	$d_{xz} \rightarrow \pi_{\text{NO}}^*$			313.4	3.96	0.0029
H→2→L+3	$d_{yz} \rightarrow \pi_{\text{NO}}^*$			312.7	3.97	0.0019

mixed character: LMCT ($\pi_{\text{Ph}} \rightarrow d$, $\pi_{\text{Br}} \rightarrow d$), MLCT ($d \rightarrow \pi_{\text{Ph}}^*$, $d \rightarrow \pi_{\text{NO}}^*$) and LLCT ($\pi_{\text{Br}} \rightarrow \pi_{\text{Ph}}^*$) character.

4. Supplementary data

Supplementary data are available from the CCDC, 12 Union Road, Cambridge CB2 1EZ, UK on request, quoting the depositions numbers: 235798 ([ReBr₃(MeCN)(dppe)]) and 235799 ([ReBr₃(NO)(dppe)]_{0.57}[ReOBr₃(dppe)]_{0.47}).

Acknowledgements

The authors thank G.Jakob from University of Mainz for magnetic measurement.

Crystallographic study was financed by funds allocated by the Ministry Of Scientific Research and Information Technology to the Institute of General and Ecological Chemistry, Technical University of Łódź.

The GAUSSIAN03 calculations were carried out in the Wrocław Centre for Networking and Supercomputing, WCSS, Wrocław, Poland under calculational grant No 51/96.

References

- [1] B.N. Storhoff, H.C. Lewis, *Coord. Chem. Rev.* 23 (1977) 1.
- [2] G.M. Bancroft, R.E.B. Garrod, A.G. Maddock, M.J. Mays, B.E. Prater, *J. Am. Chem. Soc.* 94 (1972) 647.
- [3] R.A. Brown, G.R. Dobson, *Inorg. Chim. Acta* 6 (1972) 65.
- [4] R.H.T. Bleijerveld, K. Vrieze, *Inorg. Chim. Acta* 19 (1976) 195.
- [5] J. Chantler, P.E. Fanwick, R.A. Walton, *J. Organomet. Chem.* 604 (2000) 219.
- [6] R.A. Michelin, M. Mozzon, R. Bertani, *Coord. Chem. Rev.* 147 (1996) 299.
- [7] W. Kaim, M. Moscherosch, *Coord. Chem. Rev.* 129 (1994) 157.
- [8] M.C. Fátima, G. da Silva, J.J.R.F. da Silva, A.J.L. Pombeiro, *J. Organomet. Chem.* 526 (1996) 237.
- [9] J. Chantler, P.E. Fanwick, R.A. Walton, *Inorg. Chim. Acta* 305 (2000) 215.
- [10] J.O. Dzięgielewski, K. Flipepek, B. Machura, *Polyhedron* 14 (1995) 555.
- [11] J.O. Dzięgielewski, B. Machura, J. Marek, *Polyhedron* 15 (1996) 3713.
- [12] J.O. Dzięgielewski, B. Machura, T.J. Bartczak, *Polyhedron* 15 (1996) 2813.
- [13] T.J. Bartczak, W. Czurak, J.O. Dzięgielewski, B. Machura, *Polish J. Chem.* 72 (1998) 633.
- [14] J.O. Dzięgielewski, B. Machura, T. Kupka, T.J. Bartczak, W. Czurak, *Polish J. Chem.* 72 (1998) 1009.
- [15] J.O. Dzięgielewski, B. Machura, T.J. Bartczak, W. Czurak, J. Kusz, J. Warczewski, *J. Coord. Chem.* 48 (1999) 125.
- [16] T.J. Bartczak, W. Czurak, J.O. Dzięgielewski, B. Machura, A. Jankowska, J. Kusz, J. Warczewski, *Polyhedron* 18 (1999) 2313.
- [17] T.J. Bartczak, W. Czurak, J.O. Dzięgielewski, B. Machura, J. Kusz, J. Warczewski, *Polish J. Chem.* 74 (2000) 265.
- [18] T.J. Bartczak, W. Czurak, J.O. Dzięgielewski, B. Machura, A. Jankowska, J. Kusz, J. Warczewski, *J. Coord. Chem.* 52 (2001) 361.
- [19] B. Machura, J.O. Dzięgielewski, S. Michalik, T.J. Bartczak, R. Kruszynski, *J. Kusz, Polyhedron* 21 (2002) 2617.
- [20] B. Machura, J.O. Dzięgielewski, R. Kruszynski, T.J. Bartczak, J. Kusz, *Polyhedron* 22 (2003) 2573.
- [21] B. Machura, J.O. Dzięgielewski, J. Kusz, *Polish J. Chem.* 77 (2003) 519.
- [22] R. Rossi, A. Duatti, L. Magon, U. Casellato, R. Graziani, L. Tonialo, *J. Chem. Soc., Dalton Trans.* 1982; 1949.
- [23] S. Hirata, M. Head-Gordon, *Chem. Phys. Lett.* 302 (1999) 375.
- [24] R. Andreu, J. Orduna, J. Garín, *Tetrahedron* 57 (2001) 1358.
- [25] E. Broclawik, T. Borowski, *Chem. Phys. Lett.* 339 (2001) 433.
- [26] M.J. Calhorda, M.G.B. Drew, V. Félix, L.P. Fonseca, C.A. Gamelas, S.S.M.C. Godinho, I.S. Gonçalves, E. Hunstock, J.P. Lopes, A.J. Parola, F. Pina, C.C. Romão, A.G. Santos, *J. Organomet. Chem.* 632 (221) (2001) 94.
- [27] A. Crespo, A.G. Turjanski, D.A. Estrin, *Chem. Phys. Lett.* 365 (2002) 15.
- [28] M.C. Aragoni, M. Arca, T. Cassano, C. Denotti, F.A. Devillanova, F. Isaia, V. Lippolis, D. Natali, L. Niti, M. Sampietro, R. Tommasi, G. Verani, *Inorg. Chem. Commun.* 5 (2002) 869.
- [29] P. Romaniello, F. Lejl, *Chem. Phys. Lett.* 372 (2003) 51.
- [30] P. Norman, P. Cronstrand, J. Ericsson, *Chem. Phys.* 285 (2002) 207.
- [31] J. Bossert, N.B. Amor, A. Strich, C. Daniel, *Chem. Phys. Lett.* 342 (2001) 617.
- [32] C.E. Powell, M.P. Cifuentes, A.M. McDonagh, S.K. Hurst, N.T. Lucas, C.D. Delfs, R. Stranger, M.G. Humphrey, S. Houbrechts, I. Asselberghs, A. Persoons, D.C.R. Hockless, *Inorg. Chim. Acta* 352 (2003) 9.
- [33] J.P. Morral, C.E. Powell, R. Stranger, M.P. Cifuentes, M.G. Humphrey, G.A. Heath, *J. Organomet. Chem.* 670 (2003) 248.
- [34] P. Romaniello, F. Lejl, *J. Mol. Struct. Theochem.* 636 (2003) 23.
- [35] G. Rouschias, G. Wilkinson, *J. Chem. Soc. A* 1966; 465.
- [36] STOE & Cie (1999). X-RED. Version 1.18. STOE & Cie GmbH, Darmstadt, Germany.
- [37] G.M. Sheldrick, *Acta Crystallogr.* A46 (1990) 467.
- [38] G.M. Sheldrick, *SHELXL97*. Program for the Solution and Refinement of Crystal Structures. University of Göttingen, Germany (1997).
- [39] G.M. Sheldrick, *SHELXTL*: release 4.1 for Siemens Crystallographic Research Systems (1990).
- [40] M.J. Frisch, G.W. Trucks, H.B. Schlegel, G.E. Scuseria, M.A. Robb, J.R. Cheeseman, J.A. Montgomery, Jr., T. Vreven, K.N. Kudin, J.C. Burant, J.M. Millam, S.S. Iyengar, J. Tomasi, V. Barone, B. Mennucci, M. Cossi, G. Scalmani, N. Rega, G.A. Petersson, H. Nakatsuji, M. Hada, M. Ehara, K. Toyota, R. Fukuda, J. Hasegawa, M. Ishida, T. Nakajima, Y. Honda, O. Kitao, H. Nakai, M. Klene, X. Li, J.E. Knox, H.P. Hratchian, J.B. Cross, C. Adamo, J. Jaramillo, R. Gomperts, R.E. Stratmann, O. Yazyev, A.J. Austin, R. Cammi, C. Pomelli, J.W. Ochterski, P.Y. Ayala, K. Morokuma, G.A. Voth, P. Salvador, J.J. Dannenberg, V.G. Zakrzewski, S. Dapprich, A.D. Daniels, M.C. Strain, O. Farkas, D.K. Malick, A.D. Rabuck, K. Raghavachari, J.B. Foresman, J.V. Ortiz, Q. Cui, A.G. Baboul, S. Clifford, J. Cioslowski, B.B. Stefanov, G. Liu, A. Liashenko, P. Piskorz, I. Komaromi, R.L. Martin, D.J. Fox, T. Keith, M.A. Al-Laham, C.Y. Peng, A. Nanayakkara, M. Challacombe, P.M.W. Gill, B. Johnson, W. Chen, M.W. Wong, C. Gonzalez, J.A. Pople, *GAUSSIAN 03*, Revision B.03, Gaussian, Inc., Pittsburgh, PA, 2003.
- [41] A.D. Becke, *J. Chem. Phys.* 98 (1993) 5648.
- [42] C. Lee, W. Yang, R.G. Parr, *Phys. Rev. B* 37 (1988) 785.
- [43] M.E. Casida, in: J.M. Seminario (Ed.), *Recent Developments and Applications in Modern Density Functional Theory, Theoretical and Computational Chemistry* vol. 4, Elsevier, Amsterdam, 1996.
- [44] P.J. Hay, W. R. Wadt, *J. Chem. Phys.* 82 (1985) 299.
- [45] G.R. Desiraju, T. Steiner, *The Weak Hydrogen Bond in Structural Chemistry and Biology*, Oxford University Press, Oxford, UK, 1999.
- [46] G. Ciani, D. Giusto, M. Manassero, M. Sansoni, *J. Chem. Soc., Dalton Trans.* 1975; 2156.

- [47] M. Davis, F. Belanger-Gariepy, D. Zargarian, A.L. Beauchamp, *Acta Crystallogr. C* 53 (1997) 428.
- [48] X.L.R. Fontaine, E.H. Fowless, T.P. Layzell, B.L. Shaw, M. Thornton-Pett, *J. Chem. Soc., Dalton Trans.* 1991; 1519.
- [49] Y. Wang, F.J.J.R. da Silva, A.J.L. Pombeiro, M.A. Pellinghelli, A. Tiripicchio, *J. Organomet. Chem.* 430 (1992) C56.
- [50] M. O'Keeffe, N.E. Brese, *Acta Cryst. B* 47 (1997) 192.
- [51] M. O'Keeffe, N.E. Brese, *J. Am. Chem. Soc.* 113 (1991) 3226.
- [52] I.D. Brown, Bond-Length–Bond-Valence Relationship in Inorganic Solids in Structure correlation, part III, in: H.B. Burgi, J.D. Dunitz (Eds.), VCH publishers, Weinheim/New York, 1994, pp. 405–429.
- [53] L. Sieron, M. Bukowska-Strzyzewska, *Acta Cryst. C* 55 (1999) 1230.
- [54] B. Swanson, D.F. Shriver, J.A. Ibers, *Inorg. Chem.* 8 (1969) 2182.
- [55] J.M. Mayer, *Inorg. Chem.* 27 (1988) 3899.
- [56] R. Rossi, A. Marchi, L. Marvelli, L. Magon, M. Peruzzini, U. Casellato, R. Graziani, *Inorg. Chim. Acta* 204 (1993) 63.
- [57] B.J. Coe, S.J. Glenwright, *Coord. Chem. Rev.* 203 (2000) 5.
- [58] G. Rouschias, G. Wilkinson, *J. Chem. Soc. A* 1967; 993.
- [59] R.R. Conry, J.M. Mayer, *Inorg. Chem.* 29 (1990) 4862.
- [60] C. Pearson, A.L. Beauchamp, *Inorg. Chim. Acta* 237 (1995) 13.
- [61] B.L. Haymore, I.A. Ibers, *Inorg. Chem.* 14 (1975) 3060.
- [62] J.E. Fergusson, *Coord. Chem. Rev.* 1 (1966) 459.
- [63] A. Earnshaw, B.N. Figgis, J. Lewis, R.D. Peacock, *J. Chem. Soc.* 1961; 3132.
- [64] V.S. Sergienko, *Koord. Khim.* 20 (1994) 932.